

Isotopic trends of quasifission and fusion-fission in the reactions $^{48}\text{Ca}+^{239,244}\text{Pu}$

Lu Guo^{1,2,*}, Caiwan Shen³, Chong Yu⁴, and Zhenji Wu⁴

¹*School of Nuclear Science and Technology, University of Chinese Academy of Sciences, Beijing 100049, China*

²*Institute of Theoretical Physics, Chinese Academy of Sciences, Beijing 100190, China*

³*School of Science, Huzhou University, Huzhou 313000, China and*

⁴*School of Physics, University of Chinese Academy of Sciences, Beijing 100049, China*

(Dated: March 17, 2022)

Background: Quasifission and fusion-fission are primary mechanisms to prevent the production of superheavy elements. The recent experimental measurements reveal that the fusion-evaporation cross section in the $3n$ reaction channel of $^{48}\text{Ca}+^{239}\text{Pu}$ is 50 times lower than using ^{244}Pu as target nucleus [Phys. Rev. C 92, 034609 (2015)]. However, the precise mechanisms of this remarkable isotopic dependence are not well understood.

Purpose: To understand the experimental observation of the rapid decrease of stability of superheavy nuclei as the neutron number decreases, the theoretical studies of quasifission and fusion-fission in connection with experimental production for $Z=114$ flerovium isotopes are required to investigate the possible differences in reaction mechanisms induced by these two targets.

Methods: We propose an approach called TDHF+HIVAP to take into account both the evolution of dinuclear system and the deexcitation of compound nucleus, which combines the microscopic time-dependent Hartree-Fock (TDHF) method for the fusion and quasifission dynamics with the statistical evaporation model HIVAP for fusion-fission dynamics.

Results: Fusion is observed for both reactions $^{48}\text{Ca}+^{239,244}\text{Pu}$ with the side orientation the deformed target nucleus, while quasifission dynamics is observed for the tip orientation. The nuclear contact times, masses and charges as well as the kinetic energies of the fragments, and the mass-angle distribution strongly depend on the colliding energy, impact parameter, and deformation orientation. The quantum shell effect displays a crucial role in both the quasifission and the fusion-fission processes. The quasifission is considerably reduced and the survival probability is enhanced around one order of magnitude in the reaction using ^{244}Pu target as compared to the ^{239}Pu case.

Conclusions: The studies by using TDHF+HIVAP method well account for the experimental observations and the present method clearly shows its applicability in the reaction mechanisms of quasifission and fusion-fission dynamics. The experimental and theoretical results encourage the use of neutron-rich targets for the production of new superheavy elements.

I. INTRODUCTION

The creation of superheavy elements (SHEs) is one of the most challenging research topics in nuclear physics. SHEs up to proton number $Z = 118$ have been experimentally produced in fusion-evaporation reactions, either using ^{208}Pb (or ^{209}Bi) as the target in cold fusion, or ^{48}Ca -induced hot fusion colliding with the actinide nuclei. However, the SHEs produced so far in the experiments are far from the long-lived stability island, which was predicted by many theoretical approaches [1–3], locating at the neutron magic number $N = 184$ and proton magic number $Z = 114 - 126$ as a result of new shell closures. The existence of the stability island is supported by the observed increase of stability of heavier isotopes approaching to the predicted magic number $N = 184$ [4–6].

The entrance channel dynamics is critical for SHE formation. In heavy-ion collisions, capture reaction produces a dinuclear system. The shape evolution of this initial fragile dinucleus (either fusion or quasifission) is determined by the dynamical dissipation from the collective

kinetic energy to internal degrees of freedom. The dinucleus system may evolve to an equilibrated compound nucleus in fusion process. Alternatively it can also break apart, characterized by the massive nucleon transfer and contact time longer than 5 zs. This process is known as quasifission (QF) [7–9]. For light and medium-mass systems typically with $Z_p Z_t < 1600$, the compound nucleus will be formed once the projectile is captured by the target. For heavy systems producing SHE, however, the fusion probability is dramatically reduced by the quasifission. Furthermore, even if the compound nucleus survives against quasifission, the fusion-fission (FF) has very large probability to happen due to its excitation. Hence, the production cross section forming SHE is substantially reduced by the quasifission and fusion-fission processes.

To produce the new SHEs and heavier isotopes of known SHE experimentally, the optimal target-projectile combination and bombarding energy should be chosen to have the highest residue cross sections for the desired SHE. Experimental measurements indicate an increase of residue cross sections for the reactions involving more neutron-rich nuclei [10–12]. From the theoretical point of view, the enhancement of residue cross section in the reactions with neutron-rich target could arise from the decrease of QF and FF probability. However, the precise mechanisms, especially for the interplay between the

* luguo@ucas.ac.cn

QF and FF process, are not well understood. The dependence of QF on the neutron richness of compound nucleus is supported by the recent experimental measurements of mass-angle distributions [13–16]. In particular, the recent studies of QF show a great promise for a deep insight of reaction mechanism. Meanwhile QF dynamics may be affected by many variables, e.g., collision energy [17, 18], deformation and orientation [19, 20], shell structure [21, 22] of the colliding nuclei, and neutron richness of compound nuclei [23]. Besides the competition between fusion and quasifission, the competition between the neutron emission and fission of the excited compound nucleus is also crucial for the synthesis of SHEs. To understand the complex interplay of these dynamical processes, it is required to carry out the theoretical studies.

Various theoretical models, including both the macroscopic models [24–31] and the microscopic approaches [32–36], have been developed to account for the experimental observations. Although the macroscopic model may well reproduce the experimental data, a need for external parameters and a lack of dynamical effect restrict its predictive power for reactions where no experimental data are available. In present study, we combine the microscopic time-dependent Hartree-Fock (TDHF) approach with the statistical evaporation model HIVAP to investigate the effect of neutron richness on the QF and FF dynamics. TDHF approach provides a profound understanding of nuclear dynamics, as seen from the recent applications in fusion [37–47], quasifission [48–52], transfer reaction [53–60], fission [61–66], deep inelastic collisions [67–75], and resonances dynamics [76–81]. The statistical evaporation model HIVAP [24, 82] is adopted to take into account the deexcitation process including both fission and particle evaporation. We will show that the fission barrier of compound nucleus, dominated mainly by the quantum shell effect, plays significant effect on the fusion-fission process in the present systems.

This article is organized as follows. In Sec. II TDHF approach with Skyrme energy functional and fusion-evaporation dynamics are briefly recalled. Section III presents the theoretical analysis of the influence of neutron rich target in the QF and FF dynamics for the reactions $^{48}\text{Ca} + ^{239,244}\text{Pu}$. A summary is given in Sec. IV.

II. THEORETICAL FRAMEWORK

In TDHF approach the many-body wave function $\Psi(\mathbf{r}, t)$ is approximated as a single Slater determinant composed by the single-particle states $\phi_\lambda(\mathbf{r}, t)$

$$\Psi(\mathbf{r}, t) = \frac{1}{\sqrt{N!}} \det\{\phi_\lambda(\mathbf{r}, t)\}, \quad (1)$$

and this form is kept at all times in the dynamical evolution. This approximation leads to the omission of two-body nucleon-nucleon correlations. By taking the varia-

tion of time-dependent action

$$S = \int_{t_1}^{t_2} dt \langle \Psi(\mathbf{r}, t) | H - i\hbar \partial_t | \Psi(\mathbf{r}, t) \rangle \quad (2)$$

with respect to the single-particle states, one may obtain a set of nonlinear coupled TDHF equations in the multidimensional spacetime phase space

$$i\hbar \frac{\partial}{\partial t} \phi_\lambda(\mathbf{r}, t) = h \phi_\lambda(\mathbf{r}, t), \quad (3)$$

where h is the HF single-particle Hamiltonian. It describes the time evolution of the single-particle wave functions in a mean field. The set of nonlinear TDHF equations have been solved on three-dimensional coordinate space without any symmetry restrictions and with much more accurate numerical methods.

Most TDHF calculations have been done with Skyrme effective interaction [83]. It is natural to represent the Skyrme force with the energy density functional (EDF), in which the total energy of the system

$$E = \int d^3r \mathcal{H}(\rho, \tau, \mathbf{j}, \mathbf{s}, \mathbf{T}, J; \mathbf{r}) \quad (4)$$

is expressed as an integral of the energy functional. The number density ρ , kinetic density τ , current density \mathbf{j} , spin density \mathbf{s} , spin-kinetic density \mathbf{T} , and spin-current pseudotensor density J are obtained as a sum over single-particle wave functions. The Skyrme EDF is then expressed as

$$\begin{aligned} \mathcal{H} = \mathcal{H}_0 + \sum_{t=0,1} \left\{ A_t^s \mathbf{s}_t^2 + A_t^{\Delta s} \mathbf{s}_t \cdot \Delta \mathbf{s}_t \right. \\ \left. + A_t^T \left(\mathbf{s}_t \cdot \mathbf{T}_t - \sum_{\mu, \nu=x}^z J_{t,\mu\nu} J_{t,\mu\nu} \right) \right\}, \end{aligned} \quad (5)$$

where \mathcal{H}_0 is the simplified Skyrme functional used in Sky3D code [84] and most TDHF calculations. For the definition of coupling constants A , see Ref. [85]. Due to the computational complexity, various approximations to Skyrme EDF have been employed in TDHF calculations, which restrict the number of degrees of freedom accessible during a collision, and hence the nature and degree of dissipation dynamics. For instance, the inclusion of spin-orbit interaction [86] solved an early conflict between TDHF predictions and experimental observation, and turned out to play an important role in fusion and dissipation dynamics [67, 70]. The time-odd terms appearing in Eq. (5) are also shown to be non-negligible in heavy-ion collisions [38]. Our HF and TDHF codes contain all of the time-even and time-odd terms in the energy functional and don't impose the time-reversal invariance, which allow us to compute directly the odd system, such as those studied here, without resorting to the filling approximation. As pointed out in Refs. [72, 85], the terms containing the gradient of spin density may cause the spin

instability both in nuclear structure and reaction studies, so we set $A_t^{\Delta s} = 0$ in our calculations.

In fusion-evaporation reaction, the production cross section for the superheavy evaporation residues (ER) can be defined as

$$\sigma_{\text{ER}} = \sum_{J=0}^{\infty} \sigma_{\text{cap}}(E_{\text{c.m.}}, J) P_{\text{fus}}(E^*, J) W_{\text{sur}}(E^*, J), \quad (6)$$

where σ_{cap} is the capture cross section for the projectile and target to come together, P_{fus} is the fusion probability of dinuclear system against QF, and W_{sur} is the survival probability of compound nucleus against FF. Fusion occurs when the collective kinetic energy is entirely converted into the internal excitation of a well-defined compound nucleus. Traditionally, the fusion cross section is given by

$$\sigma_{\text{fus}}(E_{\text{c.m.}}) = \sum_{J=0}^{\infty} \sigma_{\text{cap}}(E_{\text{c.m.}}, J) P_{\text{fus}}(E^*, J). \quad (7)$$

Since TDHF theory describes the collective motion of fusion dynamics in terms of semi-classical trajectories, the sub-barrier tunneling of the many-body wave function can't be included in TDHF. Consequently, the fusion cross section can be estimated by the quantum sharp-cutoff formula [87]

$$\sigma_{\text{fus}}(E_{\text{c.m.}}) = \frac{\pi \hbar^2}{2\mu E_{\text{c.m.}}} [(l_{\text{max}} + 1)^2 - (l_{\text{min}} + 1)^2], \quad (8)$$

where μ is the reduced mass of the system and $E_{\text{c.m.}}$ the initial center-of-mass (c.m.) energy. The quantities l_{max} and l_{min} denote the maximum and minimum orbital angular momentum for which fusion happens.

In the production of superheavy elements, the excited compound nucleus may undergo the deexcitation process, which is dominated by fission barrier and neutron evaporation. The survival probability of compound nucleus W_{sur} in Eq. (6) for x neutron emissions is written as

$$W_{\text{sur}}(xn) = \prod_{i=1}^x P_{in}, \quad (9)$$

where P_{in} is the probability of i -th neutron emission and given by the statistical evaporation model [88, 89]

$$P_{in} = \frac{\Gamma_{in}}{\Gamma_{in} + \Gamma_{if}}, \quad (10)$$

with Γ_{in} the i -th neutron evaporation width and Γ_{if} the i -th fission width. In the numerical calculations of present work, the HIVAP code [24, 82] is adopted to calculate the survival probability W_{sur} .

III. RESULTS

TDHF approach has recently demonstrated its feasibility and success in fusion and quasifission dynamics [49–51], in which the theoretical investigations on the reaction

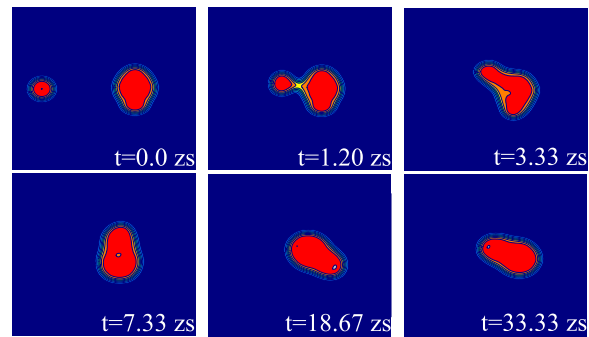


FIG. 1. (Color online) Time evolution of the mass density in the side collision of $^{48}\text{Ca} + ^{239}\text{Pu}$ at $E_{\text{c.m.}} = 204.02$ MeV and $b=1.5$ fm.

mechanism induced by the different projectiles colliding the actinide target nucleus account for the experimental observations reasonably. In present work, our goal is to investigate how the neutron richness in target nucleus affects the QF and FF dynamics in the production of SHE flerovium with the reactions $^{48}\text{Ca} + ^{239,244}\text{Pu}$. We employ the Skyrme SLy5 force [90, 91] including all of the time-odd terms in the mean-field Hamiltonian in our TDHF calculations.

In the numerical simulation, first we calculate an accurate static ground state for the projectile and target nucleus on the symmetry-unrestricted three-dimensional grid. The numerical coordinate boxes for the static HF wave functions are chosen as $24 \times 24 \times 24$ fm³ for ^{48}Ca and $32 \times 28 \times 32$ fm³ for $^{239,244}\text{Pu}$, respectively. The nucleus ^{48}Ca shows a spherical ground state and $^{239,244}\text{Pu}$ exhibits a prolate quadrupole deformation, which are in agreement with experimental data and other calculations. The correct description of the initial shape of target and projectile nucleus is important for the dynamical evolution of heavy-ion collisions. Second, we apply a boost operator on the static single-particle wave functions. The nucleus is assumed to move on a pure Coulomb trajectory until the initial distance so that the initial boost is properly treated in TDHF evolution. The time propagation is performed using a Taylor-series expansion up to the sixth order of the unitary mean-field propagator and a time step of 0.2 fm/c. For the TDHF dynamical evolution, we use a numerical box of $60 \times 28 \times 46$ fm³ and a grid spacing of 1.0 fm. The reaction is taken in x - z plane and along the collision axis x . The initial separation between the two nuclei is set to be 30 fm. The choice of these parameters assures a good numerical accuracy for all the cases studied here. The total TDHF energy and particle number are well conserved and shift less than 0.1 MeV and 0.01 in the dynamical evolution, respectively.

We first consider the reaction $^{48}\text{Ca} + ^{239}\text{Pu}$ at $E_{\text{lab}} = 245$ MeV (corresponding to $E_{\text{c.m.}} = 204.02$ MeV), which is the energy used in the Dubna experiment [12]. The time evolution of the mass density is displayed in Fig. 1, in which the symmetry axis of the prolate deformed nu-

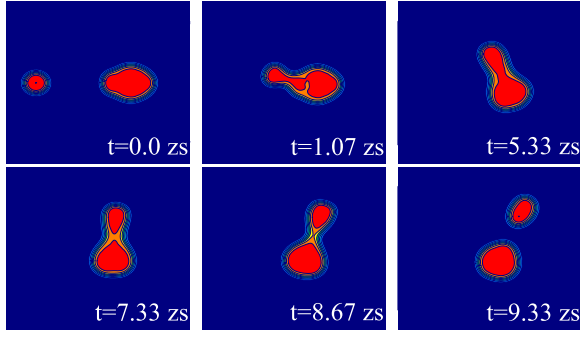


FIG. 2. (Color online) Time evolution of the mass density in the tip collision of $^{48}\text{Ca}+^{239}\text{Pu}$ at $E_{c.m.} = 204.02$ MeV and $b=2.5$ fm.

nucleus ^{239}Pu is initially set perpendicular to the internuclear axis. This is the so-called side orientation which leads to the largest contact time in central collisions [16]. We observe that TDHF calculation predicts fusion for this collision. Our definition for fusion is that an event has the contact time larger than 35 zs, and furthermore a mononuclear shape without any neck formation is required. As shown in Fig. 1, in the early stage of collision, there forms a neck between the two fragments, and the dinuclear system starts to rotate. With the time evolution, more nucleons transfer from heavy to light fragment and the neck grows into a mononuclear shape. This mononuclear system keeps its shape for enough long time and results in the fusion process.

By contrast, quasifission is observed for the same reaction, but with the tip orientation and impact parameter $b=2.5$ fm, as shown in Fig. 2. Until the neck formation, the density evolution is similar as in Fig. 1. After that, due to the competition between Coulomb repulsion and centrifugal force, the dinuclear system prolongs and then breaks in two fragments. This is the QF process which is characterized, as compared to the deep inelastic collision (DIC), by the long contact time and significant nucleon transfer. In this tip collision, the contact time is found to be 8.17 zs and roughly 30 nucleons are transferred from ^{239}Pu to ^{48}Ca . Here the contact time is calculated as the time interval in which the lowest density in the neck exceeds half of the nuclear saturation density $\rho_0/2 = 0.08 \text{ fm}^{-3}$ [16, 49, 51]. The light and heavy fragments in the exit channel are around ^{79}Ge and ^{208}Pb , respectively. The heavy fragment lying around $N = 82$ magic shell indicates that the quantum shell effect plays an important role in the QF dynamics. Such a multi-nucleon transfer is crucial to understand the dissipation dynamics in heavy-ion collisions.

We now compare the energy dependence of fusion and quasifission dynamics in the central collisions $^{48}\text{Ca}+^{239,244}\text{Pu}$. The energy range is chosen as $E_{c.m.}/V_B = 1.0-1.2$, denoted by the ratio between the colliding energy $E_{c.m.}$ and TDHF capture barrier V_B . The TDHF capture barrier is calculated for two extreme orientations of the deformed targets $^{239,244}\text{Pu}$ (tip and

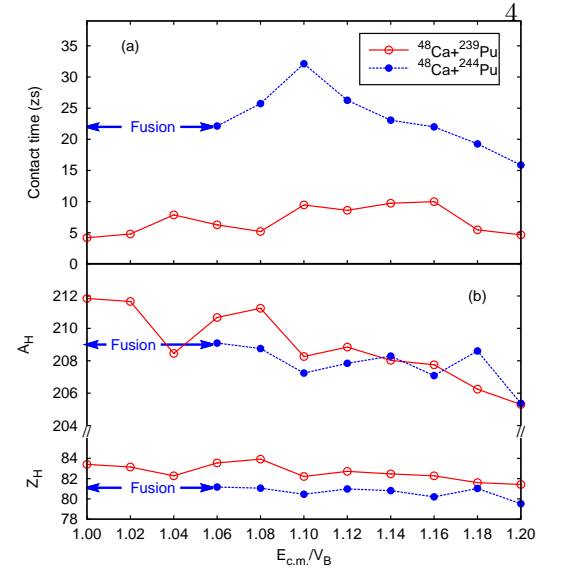


FIG. 3. (Color online) Contact time (a), mass and charge of the heavy fragments (b) as a function of $E_{c.m.}/V_B$ for the central collisions $^{48}\text{Ca}+^{239}\text{Pu}$ (open circle) and $^{48}\text{Ca}+^{244}\text{Pu}$ (solid circle) with the tip of $^{239,244}\text{Pu}$.

side). For the tip collision, the barrier is found to be 177 MeV with ^{239}Pu target and 181 MeV for ^{244}Pu , respectively. The side collision results in a significantly higher barrier of 199 MeV both for $^{239,244}\text{Pu}$ targets, as expected. TDHF calculations show that both central collisions $^{48}\text{Ca}+^{239,244}\text{Pu}$ with the side of target nuclei lead to fusion within the above energy range. Certainly, the noncentral collisions with the side orientation may show quasifission. Hence, we leave out the results for the side collisions, and the central collisions with the tip orientation are shown in Fig. 3. For the reaction $^{48}\text{Ca}+^{239}\text{Pu}$ (open circle), we observe that the contact time is within the value of 5–10 zs over a wide range of energies. But, a dramatically different behavior appears for $^{48}\text{Ca}+^{244}\text{Pu}$ (solid circle). At energies close to barrier ($E_{c.m.}/V_B = 1.0 - 1.06$), the contact time is larger than 35 zs and a mononuclear shape is kept, which is considered as fusion reaction leading to the formation of compound nucleus. As the energy increases, quasifission is observed, in which the contact time is systematically larger than the ^{239}Pu case. The long contact time of the quasifission process with the neutron-rich system relative to the neutron-deficient system have also been observed in $\text{Cr}+\text{W}$ reactions [23]. In the dynamical evolution of the neutron-rich system, the elongation of the dinuclear system is much slower and the compact configuration with mononuclear shape remains much longer, which are expected to lead to a longer contact time. These results demonstrate that the reaction with the neutron-rich target favors the fusion. In similar reactions $^{48}\text{Ca}+^{238}\text{U}$ [49] and $^{48}\text{Ca}+^{249}\text{Bk}$ [51], tip orientations are never found to lead to fusion in TDHF calculations using SLy4d force [90, 91]. This difference may

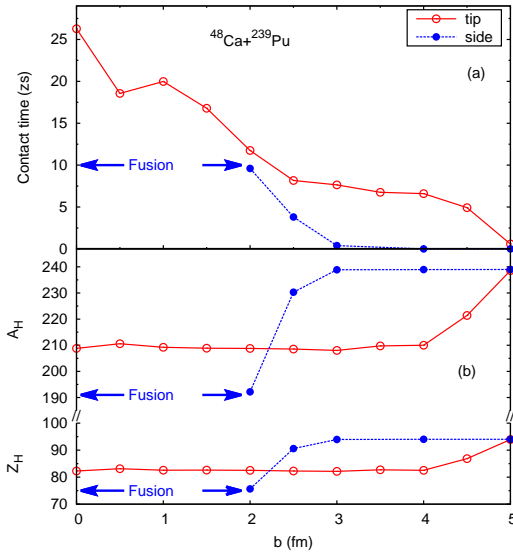


FIG. 4. (Color online) Contact time (a), mass and charge of the heavy fragments (b) as a function of impact parameter both for the tip (open circle) and side (solid circle) collisions of $^{48}\text{Ca}+^{239}\text{Pu}$ at $E_{c.m.} = 204.02$ MeV used in Dubna experiment [12].

arise from the choice of different Skyrme interaction, numerical approximations, and the shell structure of target nuclei. In particular, the influence of Skyrme interaction in QF should be examined. Since TDHF calculations for reactions leading to superheavy systems require very long CPU times, the interaction dependence of QF dynamics will be the subject of future works, which is beyond the purpose of present study.

In the lower panel of Fig. 3 are the corresponding mass and charge of the heavy fragments. We find that the transferred nucleon number is within a small variation as a function of energy. For the reaction $^{48}\text{Ca}+^{239}\text{Pu}$, the heavy QF fragments has the charge $Z_H \simeq 81.4 - 83.9$ and mass $A_H \simeq 205.3 - 211.9$ in this energy range, which is centered in the vicinity of the doubly magic nucleus ^{208}Pb . The tip collisions clearly favor the production of heavy fragments near ^{208}Pb at all energies, indicating a strong influence of the quantum shell effects. A similar effect was observed in TDHF calculations for the tip collisions using ^{238}U [49] and ^{249}Bk [51] targets. For the reaction $^{48}\text{Ca}+^{244}\text{Pu}$, the 1–2 more protons and 3–4 more neutrons are transferred on average, as compared to $^{48}\text{Ca}+^{239}\text{Pu}$, due to the charge equilibrium.

We next concentrate on the impact parameter dependence of fusion and quasifission dynamics in connection with the experimental observation, in which the isotopic dependence of measured ER cross section of Flerovium isotopes has been displayed in Ref. [12]. As stated in the Abstract of Ref. [12], the measured ER cross section in $^{239}\text{Pu}(^{48}\text{Ca}, 3n)^{284}\text{Fl}$ reaction channel are about 50 times lower than using ^{244}Pu as target nucleus. However, the precise mechanisms of this remarkable isotopic depen-

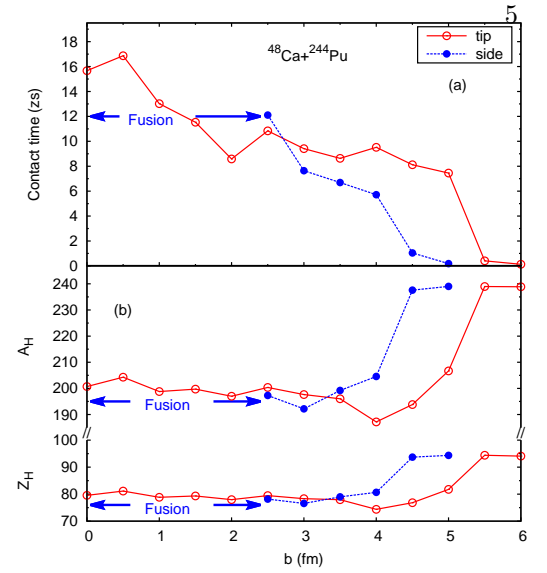


FIG. 5. (Color online) Contact time (a), mass and charge of the heavy fragments (b) as a function of impact parameter both for the tip (open circle) and side (solid circle) collisions of $^{48}\text{Ca}+^{244}\text{Pu}$ at $E_{c.m.} = 216.76$ MeV used in GSI experiment [92].

dence are not well understood yet. In the following, we will investigate how the QF and FF affect the production of SHEs.

The collision $^{48}\text{Ca}+^{239}\text{Pu}$ at $E_{lab} = 245$ MeV ($E_{c.m.} = 204.02$ MeV), which is the energy used in the Dubna experiment [12], is shown in Fig. 4. For the tip collision (open circle), the contact time is roughly linear decreasing for the impact parameter $b < 3$ fm, and then form a plateau with small variance until $b=4.0$ fm. After that, a quick decrease of contact time is observed which corresponds to the inelastic scattering. No fusion events are predicted for the tip orientation. The side collision (solid circle) shows a very different behavior as compared to the tip collision. We find that TDHF predicts fusion for $b < 2$ fm, and then a rapid drop-off within a narrow range of impact parameter 2–3 fm. At $b=3$ –5 fm the quasielastic collisions happen, characterized by the nearly zero contact time and identical fragments before and after collision. In Fig. 4(b) are the corresponding mass and charge of the heavy fragments. For the tip collision, the transferred nucleon is nearly constant in the quasifission region $b=0$ –4 fm, producing the typically heavy fragments around ^{208}Pb . This implies that the magic shell effect is also observed to be crucial as a function of impact parameter for the tip collisions. For the side collision, the transferred nucleon is proportional to the contact time. We find that only collision with the tip of ^{239}Pu produces QF fragments in the magic $Z=82$ region, while collisions with the side are the only ones that may result in fusion. These findings are consistent with the experimental observation in the collision with ^{238}U target [16].

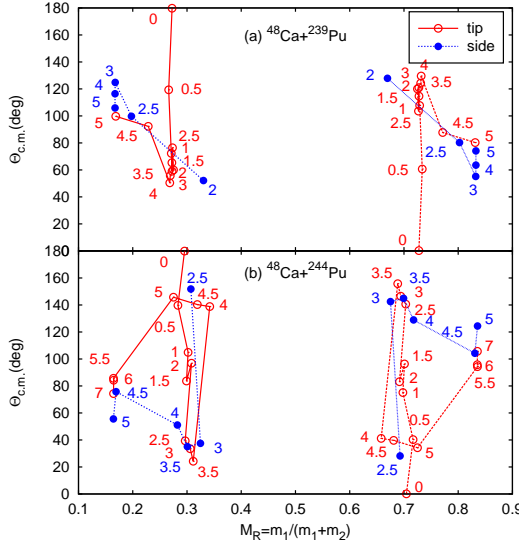


FIG. 6. (Color online) Mass-angle distribution of QF fragments both for the tip (open circle) and side (solid circle) collisions of $^{48}\text{Ca}+^{239}\text{Pu}$ at $E_{\text{c.m.}} = 204.02$ MeV (a) and $^{48}\text{Ca}+^{244}\text{Pu}$ at $E_{\text{c.m.}} = 216.76$ MeV (b). The impact parameters (in units of fm) are written next to each data point.

For comparison, the same observables for the reaction $^{48}\text{Ca}+^{244}\text{Pu}$ at energy $E_{\text{lab}} = 259.4$ MeV ($E_{\text{c.m.}} = 216.76$ MeV) used in GSI-TASCA experiment [92] are displayed in Fig. 5. For the tip collision, the contact time behaves similar as in $^{48}\text{Ca}+^{239}\text{Pu}$. The multi-nucleon transfer from the heavy to light nucleus produces the heavy fragments with the charge $Z_H \simeq 74 - 82$ and mass $A_H \simeq 192 - 212$. The heavy QF fragment is again in the vicinity of $Z=82$ magic shell. For the side orientation of ^{244}Pu nucleus, TDHF shows fusion for $b < 2.5$ fm and quasifission at $b=2.5-4$ fm, both of which are in a larger angular momentum window as compared to the ^{239}Pu case, indicating a high possibility for fusion with ^{244}Pu target.

By comparing the impact parameter dependence of fusion and quasifission dynamics between the two reactions (Fig. 4 and Fig. 5), the fusion happens in the side collision for $b < 2.0$ fm with ^{239}Pu target and $b < 2.5$ fm with ^{244}Pu . We further refine the maximum impact parameter for fusion within the precision of 0.1 fm, and find that the critical value is 1.7 fm and 2.3 fm for ^{239}Pu and ^{244}Pu cases, respectively. The fusion window is about 0.6 fm large in $^{48}\text{Ca}+^{244}\text{Pu}$, indicating that quasifission is considerably reduced as compared to the ^{239}Pu case. By using the sharp cut-off formula Eq. (8), the ratio of fusion cross section between ^{244}Pu and ^{239}Pu side collisions is roughly 1.8. One should note that the average over the orientation for the deformed target nucleus should be done if one wants to get an accurate value for this ratio.

On the other hand, the fusion-fission of compound nucleus dominated mainly by the height of fission barrier

and neutron evaporation may be sensitive to the neutron-richness of compound nucleus. This FF process is at a much longer time-scale than QF and has no memory of the entrance channel, which is beyond the scope of TDHF studies. In order to calculate the ratio of ER cross sections between ^{292}Fl ($4n$) and ^{287}Fl ($3n$), besides the ratio of their fusion cross section, we also need to calculate the ratio of their survival probability W_{sur} . However during the decay, due to the very low fission barrier B_f , the fission dominates the decay process and has several orders higher probability than the neutron emissions, and thus the W_{sur} after several neutron emissions is several orders smaller than the fusion cross section [24]. Empirically, 1 MeV larger of the B_f causes one order higher of the survival probability W_{sur} .

Some theoretical investigations indicated that ^{298}Fl could be the next double-magic nucleus after ^{208}Pb , and then one may expect more stable and larger B_f of ^{292}Fl compared to ^{287}Fl . This is confirmed by several models predicting B_f [93–95] and giving the difference of the fission barrier $\Delta B_f (= B_f(^{292}\text{Fl}) - B_f(^{287}\text{Fl}))$ around $0.82 \sim 1.98$ MeV and averaging at $B_f = 1.2$ MeV. Another simpler but frequently used B_f is approximated as $B_{\text{f(LD)}} - E_{\text{sh}}$, where $B_{\text{f(LD)}}$ is the liquid drop fission barrier and E_{sh} the shell correction energy. As an example, by adopting the $B_{\text{f(LD)}}$ from Ref. [96] and the E_{sh} from Ref. [97], corresponding to $\Delta B_f = 0.55$ MeV, the $W_{\text{sur}}(4n)$ for ^{292}Fl at $E^* = 41.7$ MeV is 8.21×10^{-8} , while the $W_{\text{sur}}(3n)$ for ^{287}Fl at $E^* = 37.7$ MeV is 5.5×10^{-9} , and hence the ratio of the survival probability for the two reactions is 14.9. Finally, involving estimated ratio of fusion cross sections, the approximate ratio of ER cross sections between the two reactions is roughly 27, close to the ratio the experimental data showing.

The mass-angle distributions (MADs) of QF fragments have been measured in experiments, which can be used to distinguish the QF from FF events. In experiments, FF fragments are usually more symmetric than in QF. In Fig. 6, we show the scattering angle as a function of the mass ratio $M_R = m_1/(m_1+m_2)$, where m_1 and m_2 are the masses of QF fragments, both for the tip (open circle) and side (solid circle) collisions of $^{48}\text{Ca}+^{239,244}\text{Pu}$. The values of impact parameters are written next to each data point. The scattering angle is calculated as the sum of the incoming and outgoing Coulomb scattering angles plus the TDHF scattering angle in the center-of-mass frame. We observe that for the tip collisions of $^{48}\text{Ca}+^{239}\text{Pu}$ the mass ratio of QF events is near $M_R = 0.22-0.27$ for light fragments and $M_R = 0.73-0.78$ for heavy fragments. At larger impact parameter $b=4.5-5$ fm for the tip collisions and $b=2.5-5$ fm for the side collision, the light fragments lying around $M_R = 0.16$ and heavy fragments $M_R = 0.84$ correspond to the quasielastic and deep-inelastic reactions. One should note that TDHF is a deterministic theory which gives only the most probable event instead of a probability distribution of various events. In the lower panel of Fig. 6, the MADs in $^{48}\text{Ca}+^{244}\text{Pu}$ show similar behavior in comparison to the $^{48}\text{Ca}+^{239}\text{Pu}$ case, except

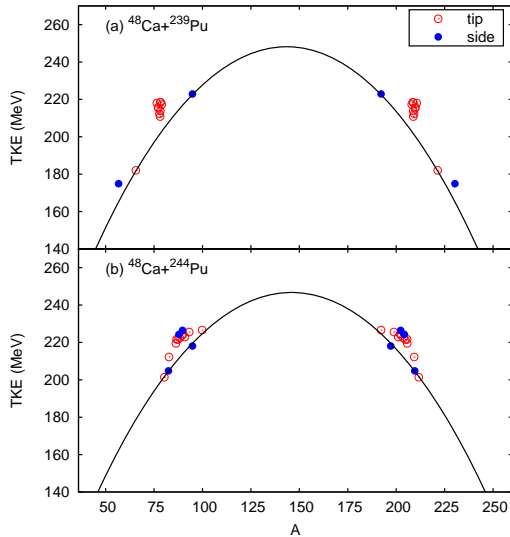


FIG. 7. (Color online) TKE-mass distribution of QF fragments both for the tip (open circle) and side (solid circle) collisions of $^{48}\text{Ca}+^{239}\text{Pu}$ at $E_{\text{c.m.}} = 204.02$ MeV (a) and $^{48}\text{Ca}+^{244}\text{Pu}$ at $E_{\text{c.m.}} = 216.76$ MeV (b). The Viola systematics (solid line) is also shown.

the larger mass ratio due to the more nucleon transfer. The MADs for the side orientation span a larger angular range in $^{48}\text{Ca}+^{244}\text{Pu}$. The detailed differences can be recognized by the values of the MADs for the specific impact parameters.

The correlation between mass and total kinetic energy (TKE) of QF fragments is another key experimental observable to distinguish the quasielastic events from fully damped events such as QF and FF. In TDHF, the TKE is calculated as the sum of kinetic energy of the fragments after the separation and the Coulomb potential energy assuming that the fragments are pointlike charges. Figure 7 shows that the TKE-mass distribution of QF fragments both for the tip (open circle) and side (solid circle) collisions of $^{48}\text{Ca}+^{239,244}\text{Pu}$. The Viola systematics (solid line) [98, 99] is also shown and has been known in good agreement with the measured TKE of experimental fission fragments. We observe that the TKE of QF fragments are distributed around the Viola systematics, indicating that most of the relative kinetic energy has been dissipated in the collision.

IV. SUMMARY

We investigate the isotopic dependence of quasifission and fusion-fission in connection with the experimental

production of superheavy flerovium isotopes for the reactions $^{48}\text{Ca}+^{239,244}\text{Pu}$ by using the microscopic TDHF approach and the statistical evaporation model HIVAP. Quasifission dynamics may be characterized by many variables, for instance, nuclear contact times, masses and charges as well as kinetic energies of the fragments, and the mass-angle distribution. We investigate the dependence of these variables on bombarding energy, impact parameter, and orientation of the deformed target. Long contact times associated with fusion are observed in both reactions with a side orientated target nucleus, whereas only quasifission dynamics is observed for the tip orientation. For the tip collisions, the quasifission fragments lying in the vicinity of the magic nucleus ^{208}Pb indicate the importance of the quantum shell effect. No quantum shell effects are observed in the collisions with the side of $^{239,244}\text{Pu}$ targets. The calculated mass-angle and TKE-mass distributions of QF fragments can be used for a direct comparison with the experimental measurements.

The quasifission in the reaction $^{48}\text{Ca}+^{244}\text{Pu}$ is found to be remarkably reduced as compared to the $^{48}\text{Ca}+^{239}\text{Pu}$ case, which leads to the ratio of fusion cross section between ^{244}Pu and ^{239}Pu side collisions roughly 1.8. The differences are attributed to the neutron-richness of target nucleus. While considering the isospin-dependence of the fission barrier, the ratio of survival probability of ^{292}Fl ($4n$) to ^{287}Fl ($3n$) is about 14.9, and thus the predicted ratio of their residue cross sections is about 27, close to the value shown by experimental data. Therefore, our studies explain the experimental observations and make clear of the precise reaction mechanisms, which may motivate the experimentalists to produce SHEs with more efficient target-projectile combinations. The present method TDHF+HIVAP demonstrates its usefulness for the microscopic reaction mechanism of quasifission and fusion-fission dynamics.

V. ACKNOWLEDGMENTS

L. G. thanks A. S. Umar for helpful discussions. This work is partly supported by NSF of China (Grants No. 11175252, 11575189, 11747312, U1732138, 11790325, 11790323), NSFC-JSPS International Cooperation Program (Grant No. 11711540016), and Presidential Fund of UCAS. The computations in present work have been performed on the High-performance Computing Clusters of SKLTP/ITP-CAS, Tianhe-1A supercomputer located in the Chinese National Supercomputer Center in Tianjin, and the C3S2 computing center in Huzhou University.

[1] M. Bender, W. Nazarewicz, and P.-G. Reinhard, Phys. Lett. B **515**, 42 (2001).

[2] P.-H. N. W. Cwiok, S. and Heenen, Nature (London) **433**, 705 (2005).

- [3] J. C. Pei, F. R. Xu, and P. D. Stevenson, *Phys. Rev. C* **71**, 034302 (2005).
- [4] Y. T. Oganessian, F. S. Abdullin, P. D. Bailey, D. E. Benker, M. E. Bennett, S. N. Dmitriev, J. G. Ezold, J. H. Hamilton, R. A. Henderson, M. G. Itkis, Y. V. Lobanov, A. N. Mezentsev, K. J. Moody, S. L. Nelson, A. N. Polyakov, C. E. Porter, A. V. Ramayya, F. D. Riley, J. B. Roberto, M. A. Ryabinin, K. P. Rykaczewski, R. N. Sagaidak, D. A. Shaughnessy, I. V. Shirokovsky, M. A. Stoyer, V. G. Subbotin, R. Sudowe, A. M. Sukhov, Y. S. Tsyganov, V. K. Utyonkov, A. A. Voinov, G. K. Vostokin, and P. A. Wilk, *Phys. Rev. Lett.* **104**, 142502 (2010).
- [5] P. A. Ellison, K. E. Gregorich, J. S. Berryman, D. L. Bleuel, R. M. Clark, I. Dragojević, J. Dvorak, P. Fallon, C. Fineman-Sotomayor, J. M. Gates, O. R. Gothe, I. Y. Lee, W. D. Loveland, J. P. McLaughlin, S. Paschalis, M. Petri, J. Qian, L. Stavsetra, M. Wiedeking, and H. Nitsche, *Phys. Rev. Lett.* **105**, 182701 (2010).
- [6] E. M. Kozulin, G. N. Knyazheva, I. M. Itkis, M. G. Itkis, A. A. Bogachev, E. V. Chernysheva, L. Krupa, F. Hanappe, O. Dorvaux, L. Stuttgé, W. H. Trzaska, C. Schmitt, and G. Chubarian, *Phys. Rev. C* **90**, 054608 (2014).
- [7] R. Bock, Y. Chu, M. Dakowski, A. Gobbi, E. Grosse, A. Olmi, H. Sann, D. Schwalm, U. Lynen, W. Müller, S. Bjørnholm, H. Esbensen, W. Wölfl, and E. Morenzoni, *Nucl. Phys. A* **388**, 334 (1982).
- [8] J. Töke, R. Bock, G. Dai, A. Gobbi, S. Gralla, K. Hildenbrand, J. Kuzminski, W. Müller, A. Olmi, H. Stelzer, B. Back, and S. B. rnholm, *Nucl. Phys. A* **440**, 327 (1985).
- [9] W. Q. Shen, J. Albinski, A. Gobbi, S. Gralla, K. D. Hildenbrand, N. Herrmann, J. Kuzminski, W. F. J. Müller, H. Stelzer, J. Tke, B. B. Back, S. Bjørnholm, and S. P. Srensen, *Phys. Rev. C* **36**, 115 (1987).
- [10] I. Dragojević, K. E. Gregorich, C. E. Düllmann, M. A. Garcia, J. M. Gates, S. L. Nelson, L. Stavsetra, R. Sudowe, and H. Nitsche, *Phys. Rev. C* **78**, 024605 (2008).
- [11] Y. T. Oganessian, V. K. Utyonkov, F. S. Abdullin, S. N. Dmitriev, R. Graeger, R. A. Henderson, M. G. Itkis, Y. V. Lobanov, A. N. Mezentsev, K. J. Moody, S. L. Nelson, A. N. Polyakov, M. A. Ryabinin, R. N. Sagaidak, D. A. Shaughnessy, I. V. Shirokovsky, M. A. Stoyer, N. J. Stoyer, V. G. Subbotin, K. Subotic, A. M. Sukhov, Y. S. Tsyganov, A. Türler, A. A. Voinov, G. K. Vostokin, P. A. Wilk, and A. Yakushev, *Phys. Rev. C* **87**, 034605 (2013).
- [12] V. K. Utyonkov, N. T. Brewer, Y. T. Oganessian, K. P. Rykaczewski, F. S. Abdullin, S. N. Dmitriev, R. K. Grzywacz, M. G. Itkis, K. Miernik, A. N. Polyakov, J. B. Roberto, R. N. Sagaidak, I. V. Shirokovsky, M. V. Shumeiko, Y. S. Tsyganov, A. A. Voinov, V. G. Subbotin, A. M. Sukhov, A. V. Sabel'nikov, G. K. Vostokin, J. H. Hamilton, M. A. Stoyer, and S. Y. Strauss, *Phys. Rev. C* **92**, 034609 (2015).
- [13] I. M. Itkis, E. M. Kozulin, M. G. Itkis, G. N. Knyazheva, A. A. Bogachev, E. V. Chernysheva, L. Krupa, Y. T. Oganessian, V. I. Zagrebaev, A. Y. Rusanov, F. Goennenwein, O. Dorvaux, L. Stuttgé, F. Hanappe, E. Vardaci, and E. de Goés Brennand, *Phys. Rev. C* **83**, 064613 (2011).
- [14] R. du Rietz, D. J. Hinde, M. Dasgupta, R. G. Thomas, L. R. Gasques, M. Evers, N. Lobanov, and A. Wakhle, *Phys. Rev. Lett.* **106**, 052701 (2011).
- [15] C. J. Lin, R. du Rietz, D. J. Hinde, M. Dasgupta, R. G. Thomas, M. L. Brown, M. Evers, L. R. Gasques, and M. D. Rodriguez, *Phys. Rev. C* **85**, 014611 (2012).
- [16] A. Wakhle, C. Simenel, D. J. Hinde, M. Dasgupta, M. Evers, D. H. Luong, R. du Rietz, and E. Williams, *Phys. Rev. Lett.* **113**, 182502 (2014).
- [17] D. J. Hinde, R. G. Thomas, R. du Rietz, A. Diaz-Torres, M. Dasgupta, M. L. Brown, M. Evers, L. R. Gasques, R. Rafiei, and M. D. Rodriguez, *Phys. Rev. Lett.* **100**, 202701 (2008).
- [18] K. Nishio, S. Mitsuoka, I. Nishinaka, H. Makii, Y. Wakabayashi, H. Ikezoe, K. Hirose, T. Ohtsuki, Y. Aritomo, and S. Hofmann, *Phys. Rev. C* **86**, 034608 (2012).
- [19] D. J. Hinde, M. Dasgupta, J. R. Leigh, J. C. Mein, C. R. Morton, J. O. Newton, and H. Timmers, *Phys. Rev. C* **53**, 1290 (1996).
- [20] E. Prasad, A. Wakhle, D. J. Hinde, E. Williams, M. Dasgupta, M. Evers, D. H. Luong, G. Mohanto, C. Simenel, and K. Vo-Phuoc, *Phys. Rev. C* **93**, 024607 (2016).
- [21] E. M. Kozulin, G. N. Knyazheva, S. N. Dmitriev, I. M. Itkis, M. G. Itkis, T. A. Loktev, K. V. Novikov, A. N. Baranov, W. H. Trzaska, E. Vardaci, S. Heinz, O. Beliuskina, and S. V. Khlebnikov, *Phys. Rev. C* **89**, 014614 (2014).
- [22] E. Prasad, D. J. Hinde, K. Ramachandran, E. Williams, M. Dasgupta, I. P. Carter, K. J. Cook, D. Y. Jeung, D. H. Luong, S. McNeil, C. S. Palshetkar, D. C. Rafferty, C. Simenel, A. Wakhle, J. Khuyagbaatar, C. E. Düllmann, B. Lommel, and B. Kindler, *Phys. Rev. C* **91**, 064605 (2015).
- [23] K. Hammerton, Z. Kohley, D. J. Hinde, M. Dasgupta, A. Wakhle, E. Williams, V. E. Oberacker, A. S. Umar, I. P. Carter, K. J. Cook, J. Greene, D. Y. Jeung, D. H. Luong, S. D. McNeil, C. S. Palshetkar, D. C. Rafferty, C. Simenel, and K. Stiefel, *Phys. Rev. C* **91**, 041602 (2015).
- [24] C. Shen, G. Kosenko, and Y. Abe, *Phys. Rev. C* **66**, 061602 (2002).
- [25] Z.-Q. Feng, G.-M. Jin, and J.-Q. Li, *Phys. Rev. C* **80**, 057601 (2009).
- [26] C. Shen, D. Boilley, Q. Li, J. Shen, and Y. Abe, *Phys. Rev. C* **83**, 054620 (2011).
- [27] J. Shen and C. Shen, *Sci. China-Phys. Mech. Astron.* **57**, 453 (2014).
- [28] L. Zhu, Z.-Q. Feng, C. Li, and F.-S. Zhang, *Phys. Rev. C* **90**, 014612 (2014).
- [29] L. Zhu, J. Su, and F.-S. Zhang, *Phys. Rev. C* **93**, 064610 (2016).
- [30] B. Wang, W. Zhao, E. Zhao, and S. Zhou, *Sci. China-Phys. Mech. Astron.* **59**, 642002 (2016).
- [31] B. Wang, K. Wen, W.-J. Zhao, E.-G. Zhao, and S.-G. Zhou, *At. Data and Nucl. Data Tables* **114**, 281 (2017).
- [32] C. Simenel, *Eur. Phys. J. A* **48**, 152 (2012).
- [33] T. Nakatsukasa, K. Matsuyanagi, M. Matsuo, and K. Yabana, *Rev. Mod. Phys.* **88**, 045004 (2016).
- [34] N. Wang, Z. Li, and X. Wu, *Phys. Rev. C* **65**, 064608 (2002).
- [35] K. Wen, F. Sakata, Z.-X. Li, X.-Z. Wu, Y.-X. Zhang, and S.-G. Zhou, *Phys. Rev. Lett.* **111**, 012501 (2013).
- [36] K. Wen, F. Sakata, Z.-X. Li, X.-Z. Wu, Y.-X. Zhang, and S.-G. Zhou, *Phys. Rev. C* **90**, 054613 (2014).
- [37] C. Simenel, P. Chomaz, and G. de France, *Phys. Rev. Lett.* **93**, 102701 (2004).

- [38] A. S. Umar and V. E. Oberacker, *Phys. Rev. C* **73**, 054607 (2006).
- [39] L. Guo and T. Nakatsukasa, *Eur. Phys. J. Web Conf.* **38**, 09003 (2012).
- [40] A. S. Umar, V. E. Oberacker, and C. J. Horowitz, *Phys. Rev. C* **85**, 055801 (2012).
- [41] C. Simenel, M. Dasgupta, D. J. Hinde, and E. Williams, *Phys. Rev. C* **88**, 064604 (2013).
- [42] A. S. Umar, C. Simenel, and V. E. Oberacker, *Phys. Rev. C* **89**, 034611 (2014).
- [43] K. Washiyama, *Phys. Rev. C* **91**, 064607 (2015).
- [44] K. Godbey, A. S. Umar, and C. Simenel, *Phys. Rev. C* **95**, 011601 (2017).
- [45] C. Simenel, A. S. Umar, K. Godbey, M. Dasgupta, and D. J. Hinde, *Phys. Rev. C* **95**, 031601 (2017).
- [46] B. Schuetrumpf and W. Nazarewicz, *Phys. Rev. C* **96**, 064608 (2017).
- [47] L. Guo, C. Simenel, L. Shi, and C. Yu, *Phys. Lett. B* **782**, 401 (2018).
- [48] C. Golabek and C. Simenel, *Phys. Rev. Lett.* **103**, 042701 (2009).
- [49] V. E. Oberacker, A. S. Umar, and C. Simenel, *Phys. Rev. C* **90**, 054605 (2014).
- [50] A. S. Umar, V. E. Oberacker, and C. Simenel, *Phys. Rev. C* **92**, 024621 (2015).
- [51] A. S. Umar, V. E. Oberacker, and C. Simenel, *Phys. Rev. C* **94**, 024605 (2016).
- [52] C. Yu and L. Guo, *Sci. China: Phys., Mech. Astron.* **60**, 092011 (2017).
- [53] K. Washiyama, S. Ayik, and D. Lacroix, *Phys. Rev. C* **80**, 031602 (2009).
- [54] C. Simenel, *Phys. Rev. Lett.* **105**, 192701 (2010).
- [55] G. Scamps and D. Lacroix, *Phys. Rev. C* **87**, 014605 (2013).
- [56] K. Sekizawa and K. Yabana, *Phys. Rev. C* **88**, 014614 (2013).
- [57] N. Wang and L. Guo, *Phys. Lett. B* **760**, 236 (2016).
- [58] K. Sekizawa and K. Yabana, *Phys. Rev. C* **93**, 054616 (2016).
- [59] G. Scamps, C. Rodríguez-Tajes, D. Lacroix, and F. Farget, *Phys. Rev. C* **95**, 024613 (2017).
- [60] K. Sekizawa, *Phys. Rev. C* **96**, 014615 (2017).
- [61] C. Simenel and A. S. Umar, *Phys. Rev. C* **89**, 031601 (2014).
- [62] G. Scamps, C. Simenel, and D. Lacroix, *Phys. Rev. C* **92**, 011602 (2015).
- [63] P. Goddard, P. Stevenson, and A. Rios, *Phys. Rev. C* **92**, 054610 (2015).
- [64] P. Goddard, P. Stevenson, and A. Rios, *Phys. Rev. C* **93**, 014620 (2016).
- [65] A. Bulgac, P. Magierski, K. J. Roche, and I. Stetcu, *Phys. Rev. Lett.* **116**, 122504 (2016).
- [66] Y. Tanimura, D. Lacroix, and S. Ayik, *Phys. Rev. Lett.* **118**, 152501 (2017).
- [67] J. A. Maruhn, P.-G. Reinhard, P. D. Stevenson, and M. R. Strayer, *Phys. Rev. C* **74**, 027601 (2006).
- [68] L. Guo, J. A. Maruhn, and P.-G. Reinhard, *Phys. Rev. C* **76**, 014601 (2007).
- [69] L. Guo, J. A. Maruhn, P.-G. Reinhard, and Y. Hashimoto, *Phys. Rev. C* **77**, 041301(R) (2008).
- [70] G.-F. Dai, L. Guo, E.-G. Zhao, and S.-G. Zhou, *Phys. Rev. C* **90**, 044609 (2014).
- [71] G.-F. Dai, L. Guo, E.-G. Zhao, and S.-G. Zhou, *Sci. China: Phys. Mech. Astron.* **57**, 1618 (2014).
- [72] P. D. Stevenson, E. B. Suckling, S. Fracasso, M. C. Barton, and A. S. Umar, *Phys. Rev. C* **93**, 054617 (2016).
- [73] L. Guo, C. Yu, L. Shi, and C. Simenel, *Eur. Phys. J. Web Conf.* **163**, 00021 (2017).
- [74] L. Shi and L. Guo, *Nucl. Phys. Rev.* **34**, 41 (2017).
- [75] A. S. Umar, C. Simenel, and W. Ye, *Phys. Rev. C* **96**, 024625 (2017).
- [76] J. A. Maruhn, P. G. Reinhard, P. D. Stevenson, J. R. Stone, and M. R. Strayer, *Phys. Rev. C* **71**, 064328 (2005).
- [77] T. Nakatsukasa and K. Yabana, *Phys. Rev. C* **71**, 024301 (2005).
- [78] A. S. Umar and V. E. Oberacker, *Phys. Rev. C* **71**, 034314 (2005).
- [79] P.-G. Reinhard, L. Guo, and J. Maruhn, *Eur. Phys. J. A* **32**, 19 (2007).
- [80] C. Simenel and P. Chomaz, *Phys. Rev. C* **80**, 064309 (2009).
- [81] S. Fracasso, E. B. Suckling, and P. D. Stevenson, *Phys. Rev. C* **86**, 044303 (2012).
- [82] C. Shen, Y. Abe, D. Boilley, G. Kosenko, and E. Zhao, *Int. J. Mod. Phys. E* **17**, 66 (2008).
- [83] T. H. R. Skyrme, *Philos. Mag.* **1**, 1043 (1956).
- [84] J. Maruhn, P.-G. Reinhard, P. Stevenson, and A. Umar, *Comput. Phys. Commun.* **185**, 2195 (2014).
- [85] T. Lesinski, M. Bender, K. Bennaceur, T. Duguet, and J. Meyer, *Phys. Rev. C* **76**, 014312 (2007).
- [86] A. S. Umar, M. R. Strayer, and P. G. Reinhard, *Phys. Rev. Lett.* **56**, 2793 (1986).
- [87] P. Bonche, B. Grammaticos, and S. Koonin, *Phys. Rev. C* **17**, 1700 (1978).
- [88] V. Weisskopf, *Phys. Rev.* **52**, 295 (1937).
- [89] N. Bohr and J. A. Wheeler, *Phys. Rev.* **56**, 426 (1939).
- [90] E. Chabanat, P. Bonche, P. Haensel, J. Meyer, and R. Schaeffer, *Nucl. Phys. A* **635**, 231 (1998).
- [91] E. Chabanat, P. Bonche, P. Haensel, J. Meyer, and R. Schaeffer, *Nucl. Phys. A* **643**, 441 (1998).
- [92] J. M. Gates, C. E. Düllmann, M. Schädel, A. Yakushev, A. Türler, K. Eberhardt, J. V. Kratz, D. Ackermann, L.-L. Andersson, M. Block, W. Brühle, J. Dvorak, H. G. Essel, P. A. Ellison, J. Even, U. Forsberg, J. Gellanki, A. Gorshkov, R. Graeger, K. E. Gregorich, W. Hartmann, R.-D. Herzberg, F. P. Heßberger, D. Hild, A. Hübnner, E. Jäger, J. Khuyagbaatar, B. Kindler, J. Krier, N. Kurz, S. Lahiri, D. Liebe, B. Lommel, M. Maiti, H. Nitsche, J. P. Omtvedt, E. Parr, D. Rudolph, J. Runke, H. Schaffner, B. Schausten, E. Schimpf, A. Semchenkov, J. Steiner, P. Thörle-Pospiech, J. Usitalo, M. Wegrzecki, and N. Wiehl, *Phys. Rev. C* **83**, 054618 (2011).
- [93] P. Möller, A. J. Sierk, T. Ichikawa, A. Iwamoto, R. Bengtsson, H. Uhrenholt, and S. Åberg, *Phys. Rev. C* **79**, 064304 (2009).
- [94] A. Staszczak, A. Baran, and W. Nazarewicz, *Phys. Rev. C* **87**, 024320 (2013).
- [95] P. Jachimowicz, M. Kowal, and J. Skalski, *Phys. Rev. C* **95**, 014303 (2017).
- [96] M. Dahlinger, D. Vermeulen, and K.-H. Schmidt, *Nucl. Phys. A* **376**, 94 (1982).
- [97] N. Wang, M. Liu, X. Wu, and J. Meng, *Phys. Lett. B* **734**, 215 (2014).
- [98] V. E. Viola, K. Kwiatkowski, and M. Walker, *Phys. Rev. C* **31**, 1550 (1985).

- [99] D. Hinde, J. Leigh, J. Bokhorst, J. Newton, R. Walsh, and J. Boldeman, Nucl. Phys. A **472**, 318 (1987).